LFT-based identification of lateral vehicle dynamics

Luca Bascetta, *Senior Member, IEEE,* and Gianni Ferretti, *Senior Member, IEEE*

***Abstract*—This paper presents a novel estimation and identification approach for lateral vehicle dynamics. The algorithm leverages on a Linear Fraction Transform (LFT) reformulation of vehicle and tyre models, allowing for a simple and computationally efficient inclusion of complex and nonlinear dynamic models, like, for example, two-wheels, four-wheels or single-track as vehicle model, and Pacejka, brush or Fiala as tyre model. As a result, this technique can be easily adopted in the development of an online identification system, able to run on a standard embedded device, implementing a flexible identification procedure that can handle different driving conditions, up to the limits of handling, different vehicle modelling approaches, and different input measurements. Experimental results demonstrate the effectiveness of the proposal, either in a persistent excitation and in a non-persistent excitation scenario.**

***Index Terms*—Lateral vehicle dynamics parameter identification, lateral vehicle dynamics state estimation, tyre model identification, LFT-based identification.**

I. Introduction

OVER the past few decades, there has been an increasing interest in the design of advanced driver assistance systems for passenger cars [1]–[4], and navigation systems for autonomous vehicles [5], aiming at improving vehicle performance, and passenger safety and comfort [6]–[8], either in standard driving conditions and at the limits of handling, as it happens, e.g., during emergency manoeuvres or in particular environmental conditions.

The majority of these navigation and assistance systems leverages on a model-based design paradigm, thus requiring the identification of lateral and longitudinal dynamics parameters, and relying on measurements or estimates of the lateral and longitudinal dynamics state variables. Furthermore, in many practical situations these parameters, especially the ones related to tyre-ground interaction, are time-varying and can suddenly change, thus asking for a continuous and fast adaption ability. As a consequence, any identification or state estimation algorithm should allow to inherently consider nonlinear dynamics, be computationally efficient supporting online estimation and parameter adaption running on a standard embedded device, i.e., without asking for an excessively high computational power, require only standard production car sensors, be robust and reliable.

On the problem of identification and estimation of lateral vehicle dynamics a huge amount of scientific literature exists, ranging from works focusing only on the identification of tyre-road friction or tyre model parameters, to complete approaches including parameter identification and state estimation.

L. Bascetta and G. Ferretti are with the Dipartimento di Elettronica, Informazione e Bioingegneria, Politecnico di Milano, Milano, Italy, e-mail: {luca.bascetta, gianni.ferretti}@polimi.it.

Focusing on works that consider only cornering stiffness identification, different approaches have been proposed in the literature, the majority of which adopts a linear tyre model. For example, in [9], [10] a method based on least squares and recursive least squares identification is proposed; in [11] center of gravity location and tyre cornering stiffnesses are simultaneously estimated; in [12] an adaptive identification of vehicle lateral and vertical dynamics parameters is introduced; and in [13] normalized tyre cornering stiffnesses are estimated in real-time, exploiting the fact that production vehicles are generally built to show some understeering characteristics.

Differently from the previous works, in [14] an individual tyre force estimation algorithm is presented, using the interacting multiple model filtering method and supporting a static nonlinear and a dynamic tyre model. Though the method is promising, and the experimental validation shows good performance, it is characterized by a significant computational complexity, hampering its practical applicability.

Even the works that consider simultaneously cornering stiffness identification and lateral dynamics estimation are mainly focused on linear tyre models. For example, in [15] a vehicle sideslip angle observer is presented, based on a nonlinear vehicle and a linear tyre model; [16] integrates an Inertial Navigation System with GPS measurements to provide an higher update rate estimate of vehicle states; [17] proposes a two-step algorithm, based on a sliding-mode observer for tyre-road forces computation and an extended Kalman filter for sideslip angle and cornering stiffness estimation; in [18] an iterative learning identification method is used to identify lateral dynamics of an agricultural vehicle; and in [19] vehicle sideslip angle and road friction are jointly estimated in real-time using an online gradient descent algorithm.

On the other side, in [20] a two-stage approach is proposed, based on an extended Kalman filter for sideslip and lateral tyre forces estimation, and nonlinear least squares for cornering stiffness identification. Thanks to the use of nonlinear least squares, either linear and nonlinear tyre models can be considered, at the expense, however, of an increased computational complexity, of potential convergence issues, and local minima. Finally, in [21] a tyre-model-less approach is presented, based on an extended Kalman filter and an adaptive neuro-fuzzy inference system, to estimate the chassis planar motion states and the tyre forces during drifting manoeuvrers. Though being general and not limited to a specific tyre model, with this approach it is not clear how to derive tyre parameters needed to design a model-based controller.

To conclude the state-of-the-art, approaches focused on tyre-road friction identification [22]–[24], possibly including also cornering stiffness identification [25], [26], and lateral dynamics estimation [27] exist, as well.

The present work proposes a solution to lateral vehicle

dynamics state estimation and parameter identification based on a Linear Fractional Transform (LFT) reformulation of the vehicle and tyre models.

The problem of model identification formulated over LFT model structures has been a subject of active research for more than ten years, see, e.g., [28]–[30], exhibiting undeniable advantages, with respect to other identification techniques, in dealing with model nonlinearities [31]. The application of this identification technique to the lateral vehicle dynamics identification and estimation problems allows to achieve all the requirements previously mentioned. In particular, LFT approach inherently supports the adoption of a complex nonlinear model, the same methodology can be thus adopted independently of the specific vehicle and tyre model, and provides a high flexibility in the selection of the measurement signals or in the introduction of further ones. Moreover, it is a computationally efficient technique that can support online estimation and parameter adaption running on a standard embedded device, and it allows to simultaneously solve not only the parameter identification, but also the state estimation problem, without any additional computational burden.

Summarising, the novel contributions of the paper are:

- at the best of the authors' knowledge, this is the first paper that proposes to formulate the lateral vehicle dynamics identification problem over an LFT formulation of the single-track model;
- the proposed approach allows to simultaneously perform lateral vehicle dynamics state estimation and parameter identification using a computationally efficient technique;
- the LFT single-track model can be easily reformulated for different tyre models, allowing the selection of the model that is most suited for each vehicle or application.

The paper is organized as follows. Section II introduces the theory supporting the LFT identification approach. In Section III, a LFT formulation of the single-track model is derived, and the application of the LFT identification approach to the problem of lateral vehicle dynamics is illustrated. Section IV describes the experimental setup used to validate the proposed identification approach. Section V shows the results of two significant experimental tests, demonstrating the effectiveness of the proposal either with a persistently exciting and with a non-persistently exciting trajectory, in standard driving conditions and at the limits of handling. Conclusions are drawn in Section VI.

II. The LFT approach to parameter identification of nonlinear systems

Consider a nonlinear, time invariant, multi-input multi-output, continuous-time system

$$\begin{aligned}\dot{\mathbf{x}}(t) &= \mathbf{f}(\mathbf{x}(t), \mathbf{u}(t), \boldsymbol{\delta}) \\ \mathbf{y}(t) &= \mathbf{g}(\mathbf{x}(t), \mathbf{u}(t), \boldsymbol{\delta})\end{aligned} \tag{1}$$

where $\mathbf{x} \in \mathbb{R}^n$, $\mathbf{y} \in \mathbb{R}^p$, are the state and noise-free output vectors, respectively, $\mathbf{u} \in \mathbb{R}^m$ is the input vector, $\boldsymbol{\delta} \in \mathbb{R}^q$ is a vector of unknown parameters, and assume as output observation equation

$$\check{\mathbf{y}}(t_k) = \mathbf{y}(t_k) + \boldsymbol{\varepsilon}(t_k)$$

where t_k, $k = 1, \ldots, N$, is the sampling instant, and $\varepsilon_i(t_k)$, $i = 1, \ldots, p$, is a discrete-time, zero-mean, white noise of variance σ_i^2.

Denote with $\boldsymbol{\delta}^o \in \mathbb{R}^q$ the true value of parameters $\boldsymbol{\delta}$.

The identification problem can be formulated as follows: given the sampled data $\{\mathbf{u}(t_k), \check{\mathbf{y}}(t_k)\}_{k=1}^N$, find the values of the unknown parameters $\boldsymbol{\delta}$ minimizing the cost function

$$J(\boldsymbol{\delta}) = \frac{1}{2N} \sum_{k=1}^{N} \mathbf{e}^T(t_k, \boldsymbol{\delta}) \mathbf{W} \mathbf{e}(t_k, \boldsymbol{\delta}) \tag{2}$$

i.e.,

$$\tilde{\boldsymbol{\delta}} = \underset{\boldsymbol{\delta} \in \mathbb{R}^q}{\arg\min}\ J(\boldsymbol{\delta}) \tag{3}$$

where

$$\mathbf{e}(t_k, \boldsymbol{\delta}) = \check{\mathbf{y}}(t_k) - \hat{\mathbf{y}}(t_k, \boldsymbol{\delta})$$

is the prediction error between the measured output $\check{\mathbf{y}}(t_k)$ and the output $\hat{\mathbf{y}}(t_k, \boldsymbol{\delta})$, predicted by model (1) using parameters $\boldsymbol{\delta}$ instead of the true parameters $\boldsymbol{\delta}^o$, and $\mathbf{W}$ is a weight matrix.

As it is well known, $\tilde{\boldsymbol{\delta}}$ is a *maximum-likelihood* estimate of the model parameters $\boldsymbol{\delta}$ for output-error plants [32], and can be determined through well-known iterative optimization procedures such as, for example, the Gauss-Newton algorithm

$$\hat{\boldsymbol{\delta}}(\nu + 1) = \hat{\boldsymbol{\delta}}(\nu) - \alpha(\nu) \hat{\mathbf{H}}^{-1} \left(\hat{\boldsymbol{\delta}}(\nu) \right) \mathbf{g} \left(\hat{\boldsymbol{\delta}}(\nu) \right) \tag{4}$$

where ν is the iteration number, $\alpha(\nu)$ is the step size, $\mathbf{g}(\boldsymbol{\delta}) : \mathbb{R}^q \to \mathbb{R}^q$ and $\hat{\mathbf{H}}(\boldsymbol{\delta}) : \mathbb{R}^q \to \mathbb{R}^{q \times q}$ are the gradient vector and a positive semi-definite approximation of the Hessian of the cost function with respect to the unknown parameters, respectively, i.e.,

$$\mathbf{g}(\boldsymbol{\delta}) = \frac{1}{N} \sum_{k=1}^{N} \mathbf{E}^T(t_k, \boldsymbol{\delta}) \mathbf{W} \mathbf{e}(t_k, \boldsymbol{\delta})$$

$$\hat{\mathbf{H}}(\boldsymbol{\delta}) = \frac{1}{N} \sum_{k=1}^{N} \mathbf{E}^T(t_k, \boldsymbol{\delta}) \mathbf{W} \mathbf{E}(t_k, \boldsymbol{\delta})$$

where $\mathbf{E}(t_k, \boldsymbol{\delta}) \in \mathbb{R}^{p \times q}$ is the Jacobian of $\mathbf{e}(t_k, \boldsymbol{\delta})$ and is given by

$$\mathbf{E}(t_k, \boldsymbol{\delta}) = \begin{bmatrix} \dfrac{\partial \mathbf{e}(t_k, \boldsymbol{\delta})}{\partial \delta_1} & \cdots & \dfrac{\partial \mathbf{e}(t_k, \boldsymbol{\delta})}{\partial \delta_q} \end{bmatrix}$$

In turn, rewriting model (1) in a Linear Fractional Transform (LFT) formulation allows for a direct computation by simulation of the gradient and approximated Hessian of the cost function [31]

$$\dot{\mathbf{x}}(t) = \mathbf{A}\mathbf{x}(t) + \mathbf{B}_1 \mathbf{w}(t) + \mathbf{B}_2 \boldsymbol{\zeta}(t) + \mathbf{B}_3 \mathbf{u}(t) \tag{5}$$

$$\mathbf{z}(t) = \mathbf{C}_1 \mathbf{x}(t) + \mathbf{D}_{11} \mathbf{w}(t) + \mathbf{D}_{12} \boldsymbol{\zeta}(t) + \mathbf{D}_{13} \mathbf{u}(t) \tag{6}$$

$$\boldsymbol{\omega}(t) = \mathbf{C}_2 \mathbf{x}(t) + \mathbf{D}_{21} \mathbf{w}(t) + \mathbf{D}_{22} \boldsymbol{\zeta}(t) + \mathbf{D}_{23} \mathbf{u}(t) \tag{7}$$

$$\mathbf{y}(t) = \mathbf{C}_3 \mathbf{x}(t) + \mathbf{D}_{31} \mathbf{w}(t) + \mathbf{D}_{32} \boldsymbol{\zeta}(t) + \mathbf{D}_{33} \mathbf{u}(t) \tag{8}$$

$$\mathbf{w}(t) = \boldsymbol{\Delta} \mathbf{z}(t) = \mathrm{diag}\{\delta_1 \mathbf{I}_{r_1}, \ldots, \delta_q \mathbf{I}_{r_q}\} \mathbf{z}(t) \tag{9}$$

$$\boldsymbol{\zeta}(t) = \boldsymbol{\Theta}(\boldsymbol{\omega}(t)) \tag{10}$$

where $\mathbf{z} \in \mathbb{R}^{n_z}$, $\boldsymbol{\omega} \in \mathbb{R}^{n_\omega}$, $\mathbf{w} \in \mathbb{R}^{n_w}$, $\boldsymbol{\zeta} \in \mathbb{R}^{n_\zeta}$ are vectors of auxiliary variables, $\mathbf{A}$, $\mathbf{B}_i$, $\mathbf{C}_i$, $\mathbf{D}_{ij}$ are 16 known constant matrices, r_i are the sizes of the corresponding identity matrices

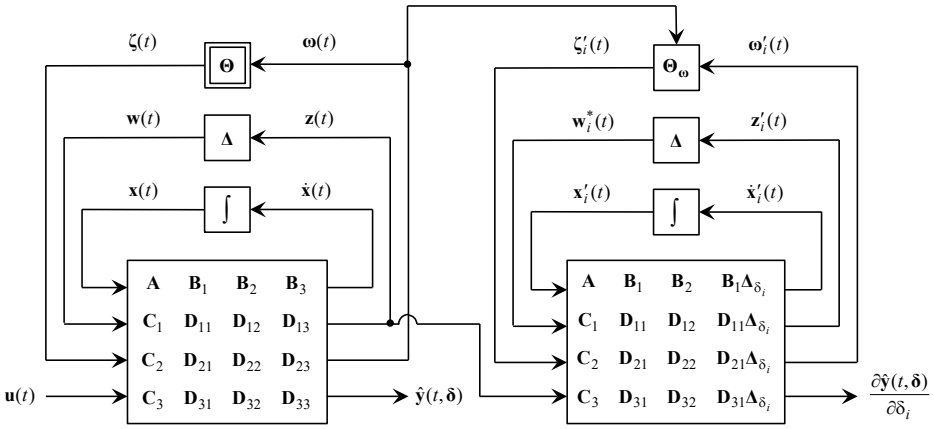

Fig. 1: Simulation scheme for the computation of the sensitivity functions.

$\mathbf{I}_{r_i}$ in the $\boldsymbol{\Delta}$ block, and $\boldsymbol{\Theta}(\boldsymbol{\omega}) : \mathbb{R}^{n_\omega} \rightarrow \mathbb{R}^{n_\zeta}$ is a known nonlinear vector function.

The model in the LFT formulation, although being formally equivalent to the original one, is now clearly divided in 3 parts:

1) a *linear* part: equations (5 – 8);
2) a *nonlinear* part: equation (10), defined by vector function $\boldsymbol{\Theta}\left(\boldsymbol{\omega}\left(t\right)\right)$;
3) an *uncertain* part: equation (9), where vector $\mathbf{z}(t)$ multiplies matrix $\boldsymbol{\Delta} = \text{diag}\{\delta_1 \mathbf{I}_{r_1}, \ldots, \delta_q \mathbf{I}_{r_q}\}$, collecting the unknown parameters.

Simulating the LFT formulation fed by the sampled input $\mathbf{u}(t_k)$ yields the predicted output $\hat{\mathbf{y}}(t_k, \boldsymbol{\delta})$ (first stage of the scheme in Figure 1).

Furthermore, the sensitivity

$$\frac{\partial \mathbf{e}(t_k, \boldsymbol{\delta})}{\partial \delta_i} = -\frac{\partial \hat{\mathbf{y}}(t_k, \boldsymbol{\delta})}{\partial \delta_i} = -\mathbf{y}'_i(t_k)$$

can be computed by sampling the output $\mathbf{y}'_i(t)$ of the following LFT system (second stage of the scheme in Figure 1)

$$\begin{aligned}
\dot{\mathbf{x}}'_i(t) &= \mathbf{A}\mathbf{x}'_i(t) + \mathbf{B}_1\mathbf{w}^*_i(t) + \mathbf{B}_2\boldsymbol{\zeta}'_i(t) + \mathbf{B}_1\boldsymbol{\Delta}_{\delta_i}\mathbf{z}(t) \\
\mathbf{z}'_i(t) &= \mathbf{C}_1\mathbf{x}'_i(t) + \mathbf{D}_{11}\mathbf{w}^*_i(t) + \mathbf{D}_{12}\boldsymbol{\zeta}'_i(t) + \mathbf{D}_{11}\boldsymbol{\Delta}_{\delta_i}\mathbf{z}(t) \\
\boldsymbol{\omega}'_i(t) &= \mathbf{C}_2\mathbf{x}'_i(t) + \mathbf{D}_{21}\mathbf{w}^*_i(t) + \mathbf{D}_{22}\boldsymbol{\zeta}'_i(t) + \mathbf{D}_{21}\boldsymbol{\Delta}_{\delta_i}\mathbf{z}(t) \\
\mathbf{y}'_i(t) &= \mathbf{C}_3\mathbf{x}'_i(t) + \mathbf{D}_{31}\mathbf{w}^*_i(t) + \mathbf{D}_{32}\boldsymbol{\zeta}'_i(t) + \mathbf{D}_{31}\boldsymbol{\Delta}_{\delta_i}\mathbf{z}(t)
\end{aligned}$$

where

$$\begin{aligned}
\boldsymbol{\Delta}_{\delta_i} &= \frac{\partial \boldsymbol{\Delta}}{\partial \delta_i} = \text{diag}\{\mathbf{0}_{r_1 \times r_1}, \ldots, \mathbf{I}_{r_i}, \ldots, \mathbf{0}_{r_q \times r_q}\} \\
\mathbf{w}^*_i(t) &= \boldsymbol{\Delta}\mathbf{z}'_i(t) \\
\boldsymbol{\zeta}'_i(t) &= \left.\frac{\partial \boldsymbol{\Theta}(\boldsymbol{\omega})}{\partial \boldsymbol{\omega}}\right|_{\boldsymbol{\omega}=\boldsymbol{\omega}(t)} \boldsymbol{\omega}'_i(t) = \boldsymbol{\Theta}_{\boldsymbol{\omega}}\left(\boldsymbol{\omega}\left(t\right)\right)\boldsymbol{\omega}'_i(t)
\end{aligned}$$

which can be rewritten as a time-variant linear system.

Further information on the implementation of the LFT-based identification algorithm can be found in [31]. A MATLAB™ Toolbox for parameter identification of nonlinear LFT models is available, as well[1].

It is also worth mentioning that, in order to deal with parameter estimation, it is essential to rewrite model (5−10) by introducing normalized unknown parameters $\bar{\delta}_i \in [-1, 1]$, as parameter δ_i varies between a maximum $\delta_i^{\max}$ and a minimum $\delta_i^{\min}$ value, as follows

$$\delta_i = \frac{(\delta_i^{\max} + \delta_i^{\min})}{2} + \frac{\bar{\delta}_i(\delta_i^{\max} - \delta_i^{\min})}{2}$$

Remark 1 (Online implementability of the identification algorithm): From an implementation point of view, the LFT-based identification algorithm can be decomposed into three steps:

1) integration of a LFT system;
2) integration of q linear sensitivity filters;
3) solution of the optimization algorithm in (3).

Concerning step (1), the integration of a LFT system can be easily implemented online, or even in a real-time system, using any fixed-step solver. The time required to perform step (2), representing the integration of q linear filters, can be considered negligible with respect to step (1) and (3). Finally, step (3) can be solved, as already mentioned in (4), using an iterative optimization procedures such as, for example, the Gauss-Newton algorithm. To meet the required time constraint, the optimization algorithm can be stopped either when the minimum is reached, or when the available time expires.

III. LFT FORMULATION OF THE SINGLE-TRACK MODEL

Though, as already mentioned in Section I, almost any nonlinear model allows for a LFT formulation, as it is common in the control and robotics literature, the longitudinal and lateral dynamics of a vehicle are here represented using the single-track approximation (Figure 2), i.e., the motion equations are developed lumping together the wheels on the same front or rear axle at its centreline, and assuming the vehicle mass is concentrated in the center of gravity, whose position with respect to the wheel axles is fixed.

Assuming that:

- ground slope, longitudinal load transfer, and pitching and rolling motions are neglected;
- sideslip and steering angle are small enough to introduce the approximations $\sin(x) \approx x$ and $\cos(x) \approx 1$;
- the vehicle is rear-wheel drive and braking forces are neglected;

[1]See https://github.com/looms-polimi/LFTSolver.

- the vehicle velocity is slowly varying, i.e., the Newton equation related to the longitudinal motion is considered at steady state;

the single-track motion model considered for parameter identification can be expressed through the following dynamical system

$$\begin{aligned} m\dot{v}_y &= F_f + F_r - m v_x r \\ I_z \dot{r} &= a F_f - b F_r \\ \dot{\psi} &= r \end{aligned} \tag{11}$$

where

- v_x and v_y are the longitudinal and lateral components of the velocity of the center of mass, respectively;
- r is the yaw rate;
- ψ is the yaw angle;
- I_z, is the yaw inertia referred to the center of gravity;
- m, is the mass;
- a and b are the distances of the vehicle center of gravity from the front and rear axles, respectively;
- F_f and F_r are the front and rear lateral forces, respectively.

The front and rear lateral forces can be represented by a linear tyre model or by a more complex, but more general, nonlinear one. To consider either standard conditions and driving at the limits of handling, a nonlinear Fiala tyre model, a variant of brush model [33], is here introduced

$$F_\star = \begin{cases} C_\star z \left(1 - \dfrac{|z|}{z_{sl_\star}} + \dfrac{z^2}{3 z_{sl_\star}^2}\right) & |z| < z_{sl_\star} \\ \mu F_{z_\star} \operatorname{sgn}(\alpha_\star) & |z| \geq z_{sl_\star} \end{cases} \tag{12}$$

where "$\star$" stands for "f" or "r", and

$$z = \tan(\alpha_\star) \qquad z_{sl_\star} = \frac{3\mu F_{z_\star}}{C_\star}$$

with $C_\star$ being the front and rear cornering stiffnesses, μ the tyre-ground friction coefficient, and $F_{z_\star}$ the tyre normal load. This load can be expressed in different ways, depending on the considered load transfer model. For the sake of simplicity, a static load is here considered, i.e.,

$$F_{z_f} = \frac{mgb}{2(a+b)} \qquad F_{z_r} = \frac{mga}{2(a+b)}$$

Front and rear slip angles $\alpha_\star$ are related to vehicle lateral dynamics by the following equations

$$\begin{aligned} \alpha_f &= -\beta - a\frac{r}{v_x} + G\gamma \\ \alpha_r &= -\beta + b\frac{r}{v_x} \end{aligned} \tag{13}$$

where γ and G are the steering angle and the steering gain, respectively, and β is the sideslip angle, defined as

$$\beta = \arctan\left(\frac{v_y}{v_x}\right) \tag{14}$$

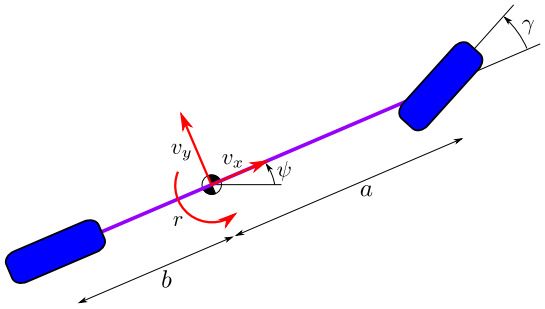

Fig. 2: Single-track vehicle model.

Model (11)-(13) can be written in the general form (1) by defining the following state, $\mathbf{x}$, output, $\mathbf{y}$, input, $\mathbf{u}$, and parameter, $\boldsymbol{\delta}$, vectors:

$$\begin{aligned} \mathbf{x} &= \begin{bmatrix} v_y & r \end{bmatrix}^T & \mathbf{y} &= \begin{bmatrix} r & a_y & \beta \end{bmatrix}^T \\ \mathbf{u} &= \begin{bmatrix} v_x & \gamma \end{bmatrix}^T & \boldsymbol{\delta} &= \begin{bmatrix} \dfrac{C_f}{m} & \dfrac{C_r}{m} & \dfrac{C_f}{I_z} \end{bmatrix}^T \end{aligned} \tag{15}$$

where a_y is the lateral acceleration, defined as follows

$$a_y = \frac{1}{m}(F_f + F_r)$$

Recalling that

$$\frac{C_r}{I_z} = \left(\frac{C_r}{m}\frac{C_f}{I_z}\right)\left(\frac{C_f}{m}\right)^{-1} = \frac{\delta_2 \delta_3}{\delta_1} \tag{16}$$

where δ_i is the i-th component of vector $\boldsymbol{\delta}$, a relevant LFT formulation is given by

$$\dot{\mathbf{x}} = \begin{bmatrix} w_1 + w_2 - \zeta_4 \\ w_3 - \dfrac{b}{a}\zeta_5 \end{bmatrix} \qquad \mathbf{z} = \begin{bmatrix} \zeta_2 \\ \zeta_3 \\ a\zeta_2 \end{bmatrix} \qquad \mathbf{w} = \begin{bmatrix} z_1\delta_1 \\ z_2\delta_2 \\ z_3\delta_3 \end{bmatrix}$$

$$\boldsymbol{\omega} = \begin{bmatrix} x_1 \\ x_2 \\ w_1 \\ w_2 \\ w_3 \\ \zeta_1 \\ u_1 \\ u_2 \end{bmatrix} \qquad \boldsymbol{\zeta} = \begin{bmatrix} \arctan\left(\dfrac{\omega_1}{\omega_7}\right) \\ \Phi(\alpha_f, z_{slf}) \\ \Phi(\alpha_r, z_{slr}) \\ \omega_2\omega_7 \\ \dfrac{\omega_4\omega_5}{\omega_3} \end{bmatrix} \qquad \mathbf{y} = \begin{bmatrix} x_2 \\ w_1 + w_2 \\ \zeta_1 \end{bmatrix}$$

where

$$\Phi(\alpha_\star, z_{sl_\star}) = \tan(\alpha_\star)\left[1 - \frac{|\tan(\alpha_\star)|}{z_{sl_\star}} + \frac{\tan^2(\alpha_\star)}{3 z_{sl_\star}^2}\right]$$

and the slip angles can be expressed as

$$\begin{aligned} \alpha_f &= -\omega_6 - a\frac{\omega_2}{\omega_7} + G\omega_8 \\ \alpha_r &= -\omega_6 + b\frac{\omega_2}{\omega_7} \end{aligned}$$

The sixteen constant matrices defining the LFT formulation of the single-track model are reported in Appendix A.

Remark 2 (Fiala model identifiability): Note that, experimental results show that in full sliding conditions, namely when lateral forces are about to saturate, a scarce identifiability

is obtained, and parameters $z_{sl_\star}$, that determine the full sliding condition, are weakly dependent on the cornering stiffness values. For these reasons, though the LFT framework would have allowed to explicitly consider the dependence of $z_{sl_\star}$ on the unknown parameters $\boldsymbol{\delta}$, it was preferred to consider $z_{sl_\star}$ as constant parameters (whose values can be computed based on nominal parameter values or, in the case of an online identification, based on the last identification results), while freezing the identification algorithm during full sliding, and when $v_x \to 0$. This choice, though possibly been suboptimal, allows to have a definitely more simple LFT form, reducing the computational burden and easing the developing of a fast online implementation. Furthermore, it allows to express the LFT form in terms of unknowns that are expressed as a ratio between the parameters one would like to identify and vehicle mass or inertia, significantly increasing the estimation quality (see Remark 3).

Remark 3 (selecting unknown parameters): It must be emphasized that cornering stiffnesses appear in the model only in ratios with inertial parameters. On one hand, an accurate estimation of C_f and C_r depends on an accurate a-priori knowledge of m and I_z; on the other hand, the four parameters C_f, C_r, m and I_z cannot be independently estimated.
As a consequence, one could directly consider the four ratios C_f/m, C_r/m, C_f/I_z, and C_r/I_z as unknown parameters, but they are still not independent, as one of them can be computed from the other three, as shown in (16).
Three ratios, namely $\delta_1 = C_f/m$, $\delta_2 = C_r/m$, and $\delta_3 = C_f/I_z$, have been therefore considered for identification, while assuming vehicle mass m as known, so that the estimated values for the cornering stiffnesses and the vehicle moment of inertia can be computed as

$$\tilde{C}_f = m\tilde{\delta}_1 \qquad \tilde{C}_r = m\tilde{\delta}_2 \qquad \tilde{I}_z = m\frac{\tilde{\delta}_1}{\tilde{\delta}_3}$$

where $\tilde{\delta}_i$ is a maximum-likelihood estimate of parameter δ_i.

Remark 4 (selecting input measurements): The identification problem in (15) has been formulated considering as measurements the physical quantities that characterize the lateral dynamics of a vehicle and, for this reason, that are more sensitive to changes in the cornering stiffnesses, i.e., the identified parameters.
It is straightforward that the measurement vector can be arbitrarily changed, adding, for example, all the measurements that are available on the vehicle. There is no guarantee, however, that adding further measurements increases the estimation quality. A typical example is represented by vehicle position measurements, provided by a GNSS system that is almost always available on a vehicle. It has been verified that, adding these measurements that, especially in urban environments, are affected by high frequency flicker noise and multi-path errors, does not increase identifiability or estimation quality.
Finally, among the selected measurements, yaw rate r and lateral acceleration a_y can be easily measured using a standard IMU, while sideslip β can be directly measured, using suitable optical sensors, or estimated using one of the many algorithms available in the literature [34].

Remark 5 (selecting tyre model): The LFT formulation of the single-track model presented in this section is based on the Fiala tyre model, as this model represents the best compromise between accuracy and complexity, at least as far as model-based control and estimation is concerned.
The LFT approach here proposed, however, allows to easily reformulate the model considering different tyre modelling techniques, without changing the identification procedure, allowing thus the selection of the tyre model that is most suited for each vehicle or application.
As an example to show this advantage, Appendix B reports the LFT formulation of the single-track model considering, as tyre model, the Pacejka magic formula.

Remark 6 (selecting model complexity): The LFT formulation of the single-track model presented in this section is based on some common simplifying assumptions, e.g., the approximations $\sin(x) \approx x$ and $\cos(x) \approx 1$. Though the results presented in Section V demonstrate that those approximations do not significantly affect the accuracy of the estimated parameters, even when driving at the limits of handling, the LFT approach allows to easily reformulate the model including those nonlinearities, without changing the identification procedure. Consequently, model complexity can be easily adapted according to application requirements.

IV. Experimental setup

A 1:10 scale car-like vehicle (Figure 3), inspired by the ones used by ETH and Georgia Institute of Technology researchers [35], [36], has been adopted to test the proposed identification algorithm.

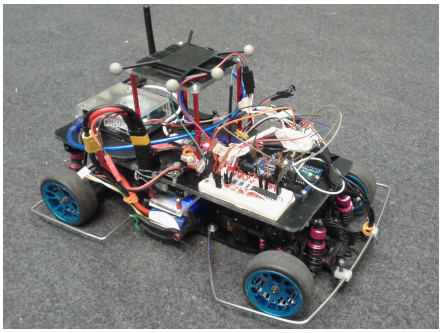

Fig. 3: The experimental platform.

The platform is a RWD vehicle, actuated by a current controlled brushless motor, and equipped with four independent suspensions and an electric steering servo along with a rear differential. The vehicle can be either manually controlled with a standard RC radio system, or can autonomously drive thanks to the installation of an embedded PC Odroid XU4 that runs a ROS control architecture. In both situations, an Arduino UNO provides a bidirectional communication with steering, propulsion, and wheel encoders.

The vehicle is equipped with an IMU, providing linear acceleration, angular velocity and attitude measurements, and a marker that allows to track vehicle position and orientation at a frequency of 100 Hz using a 12-camera OptiTrack motion

TABLE I: Steering servo actuator data

Maximum steering angle	$\pm$ 45	deg
Actuator bandwidth	14	Hz
Actuator delay	0.055	s
Pole natural frequency	87.62	rad/s
Pole damping	0.75	

TABLE II: Vehicle data

Mass	2.04	Kg
Distance of COG from front axle	0.1713	m
Distance of COG from rear axle	0.0887	m
Rubber tyres static friction coefficient	0.65	
Drifting tyres static friction coefficient	0.385	

tracking system, which has been used to estimate vehicle longitudinal and lateral velocities.

The steering servo dynamics has been identified by mounting the IMU on one of the front wheels, and by recording the yaw rate in response to a step of the angular position of the servo. Servo dynamics is well reproduced by a second order low-pass filter, whose parameters are reported in Table I.

Vehicle mass and center of gravity position have been measured with a digital scale. In particular, longitudinal position of the center of gravity has been estimated by measuring the longitudinal weight distribution, i.e., mass acting on the front and rear axle. The results are reported in Table II.

Finally, the vehicle can be equipped with two different sets of tyres, i.e., drifting tyres, characterized by an hard compound, and rubber tyres, characterized by a soft compound, and experiments are performed on a four square meter carpet used to simulate road surface. Preliminary identification experiments, measuring vehicle lateral acceleration at the center of gravity during a steady-state turning manoeuvre bringing the vehicle up to its limits of handling, have been performed in order to determine static friction coefficients associated to each set of tyres. The results are reported in Table II.

Remark 7 (validity of the scaled car experiments): Using a car model instead of a real vehicle allows to execute aggressive manoeuvres without running the risk of damaging the car or the environment, or of harming people; as otherwise it could be done only in simulation. The adoption of a scaled vehicle model is also fostered by the existence of a dynamic similitude, expressed by the Buckingham-Pi theorem [37], [38]. According to it, the solutions to the nonlinear differential equations modelling a real vehicle are proved to be identical, after accounting for the dimensional scaling of each parameter in the equations, to the solutions of the differential equations describing the scaled model. In particular, the scaled car-like vehicle here considered can be put in dynamic similitude with a Sedan car with a dimensional scaling factor of 4, i.e., a velocity of 1 m/s for the scaled car corresponds to 4 m/s for the Sedan car.

V. Experimental results

An extensive experimental campaign has been performed to validate the proposed identification approach, considering various trajectories executed on a carpet surface with the two different sets of tyres. Among the many performed experiments, results of two of them characterized by a mixed trajectory, and two by an eight shaped trajectory, where for each trajectory one experiment is executed with drifting and one with rubber tyres, are illustrated in the following.
The values of the identified parameters, that are the same for all experiments, are reported in Table III.

The measurements considered in the identification process, as explained in Section III, are yaw rate r, lateral acceleration a_y, and sideslip angle β. As introduced in Section IV, the vehicle is equipped with an IMU, lateral acceleration and yaw rate can be thus obtained, with a frequency of $100\,\text{Hz}$, from this sensor. On the other hand, vehicle pose is measured by an OptiTrack motion capture system with a frequency of $100\,\text{Hz}$, and this measure is used to compute, using a digital filter, the longitudinal and lateral vehicle velocities, v_x and v_y, and, using expression (14), sideslip angle β. Note that, the presence of outliers and discontinuities in these signals is due to measurement errors or packet loss in the OptiTrack system. Though this issue occurs only on a few samples, that can be easily removed or corrected, their presence allows to emphasise the algorithm robustness against measurement errors.
The available measurements allow to compute, thanks to relations (13), slip angles, and, solving the following linear system for each sample

$$\begin{bmatrix} a\cos(\gamma) & -b \\ \cos(\gamma) & 1 \end{bmatrix} \begin{bmatrix} F_f \\ F_r \end{bmatrix} = \begin{bmatrix} I_z \dot{r} \\ m a_y \end{bmatrix}$$

the front and read lateral forces F_f and F_r.
Finally, steering servo does not provide a measurement of the actual steering position, only the steering command, i.e., the reference value of the steering servo loop, is available. Considering, however, that steering servo dynamics are not fast enough to be considered as ideal, an estimate of the actual steer position, obtained by filtering the steer command with the second order identified steering servo dynamics (see Table I), is used in the identification process.
Summarising, in all experiments the estimation algorithm is fed with:

- vehicle commands
  - steering angle γ, obtained by filtering the steer command with the second order identified steering servo dynamics;
  - longitudinal velocity v_x, obtained differentiating the vehicle position measured by the optoelectronic system;
- vehicle measurements
  - yaw rate r and lateral acceleration a_y, measured by an IMU;
  - sideslip angle β, obtained differentiating the vehicle position measured by the optoelectronic system and applying equation (14);

and it provides an estimate of

- cornering stiffness $\tilde{C}_f$ and $\tilde{C}_r$;
- yaw inertia $\tilde{I}_z$;

TABLE III: Identified vehicle parameters

Yaw moment of inertia	0.03054	$\mathrm{Kg\,m^2}$
Front wheel cornering stiffness	25.5	$\mathrm{N/rad}$
Rear wheel cornering stiffness	51.0	$\mathrm{N/rad}$

Finally, using these parameters and the single-track model, the proposed approach allows to reconstruct the time history of slip angles α_f, α_r, lateral forces F_f, F_r, sideslip β, yaw rate r, and lateral acceleration a_y, without any further computational burden, i.e., it simultaneously performs lateral vehicle dynamics state estimation and parameter identification.

Note that, in order to properly balance the influence of the available measurements in the identification process, a simple normalization procedure has been applied

$$\mathbf{W} = \begin{bmatrix} W_1 & 0 & 0 & 0 \\ 0 & W_2 & 0 & 0 \\ 0 & 0 & \ddots & 0 \\ 0 & 0 & 0 & W_p \end{bmatrix}$$

with

$$W_i = \frac{1}{(\bar{y}_i - \underline{y}_i)^2}$$

where $\bar{y}_i$ is the highest value of the i-th output measurement, and $\underline{y}_i$ the lowest one.

A. Mixed trajectory

The first set of experiments is related to a mixed trajectory, which includes turns characterized by different turning radii and taken at low and high speed, i.e., the typical input used for parameter identification, as it is able to persistently excite all system dynamics.
An example of the input signals, i.e., vehicle speed and steer, is reported in Figures 4a and 4b for rubber tyres, and in Figures 4c and 4d for drifting tyres.

Using the available measurements and applying the procedure described in Section III, cornering stiffnesses and yaw inertia have been estimated (results are reported in Table III). Then, slip angles and lateral forces have been reconstructed. For the experiment with rubber tyres the time interval considered for identification is $[5, 20]$ seconds, while for the one with drifting tyres is $[5, 15]$ seconds.

A first validation of the identified parameters is shown in Figure 5, where the force-slip curves obtained from relation (12), using the identified values of the cornering stiffnesses, are shown together with force and slip samples reconstructed from measurements. As it can be clearly seen, either in the case of rubber (Figures 5a and 5b) and drifting (Figures 5c and 5d) tyres force-slip curves obtained with identified parameters are in good accordance with experimental data.

A second validation is based on the comparison between experimental and simulation data, where the second one are obtained simulating model (11)-(13) based on the values of the identified parameters. In particular, Figures 6 and 7 show the comparison between simulated and experimental measurements related to vehicle lateral dynamics, i.e., yaw rate, lateral acceleration and sideslip, for the case of rubber and drifting tyres, respectively. Instead, Figures 8 and 9 show the comparison between simulated and experimental lateral forces and slip angles, respectively, reconstructed from measurements as explained in Section V. It is apparent that simulation and experimental results are in very good accordance.

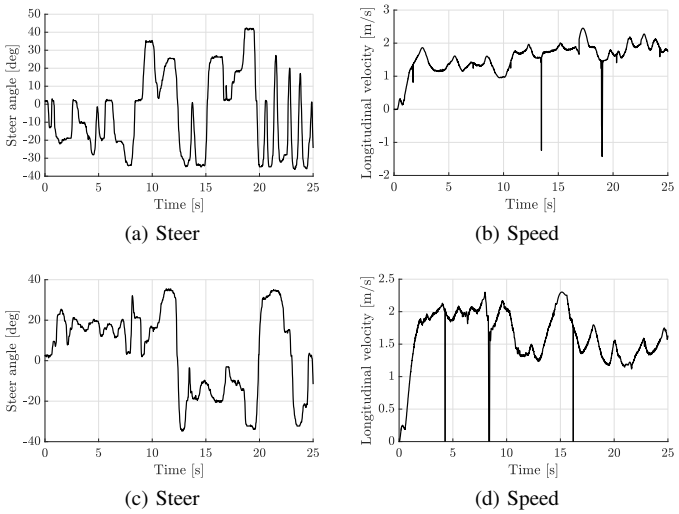

(a) Steer (b) Speed

(c) Steer (d) Speed

Fig. 4: Vehicle commands in mixed trajectory experiment with rubber (Figures 4a and 4b) and drifting (Figures 4c and 4d) tyres.

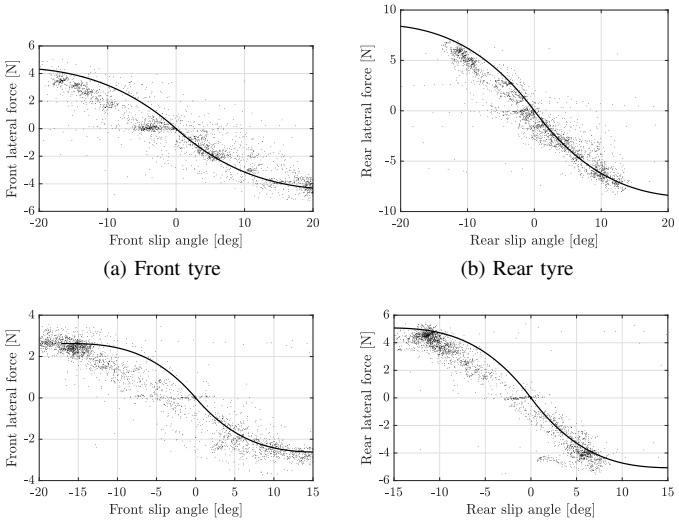

(a) Front tyre (b) Rear tyre

(c) Front tyre (d) Rear tyre

Fig. 5: Force-slip curve (estimated curve as a black solid line, experimental data as black dots) in mixed trajectory experiment with rubber (Figures 5a and 5b) and drifting (Figures 5c and 5d) tyres.

B. Eight shaped trajectory

The second set of experiments is related to an eight shaped trajectory, characterized by two curves with opposite values of yaw rate. Differently from the one presented in Section V-A,

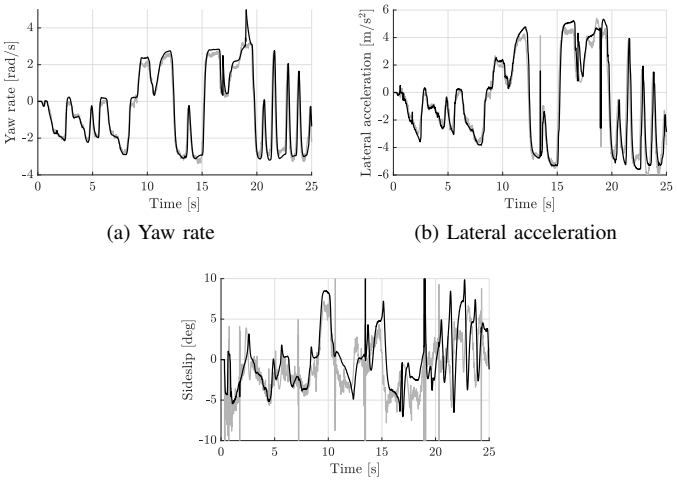

(a) Yaw rate (b) Lateral acceleration

(c) Sideslip

Fig. 6: Lateral dynamics (experimental data in grey, simulated data in black) in mixed trajectory experiment with rubber tyres.

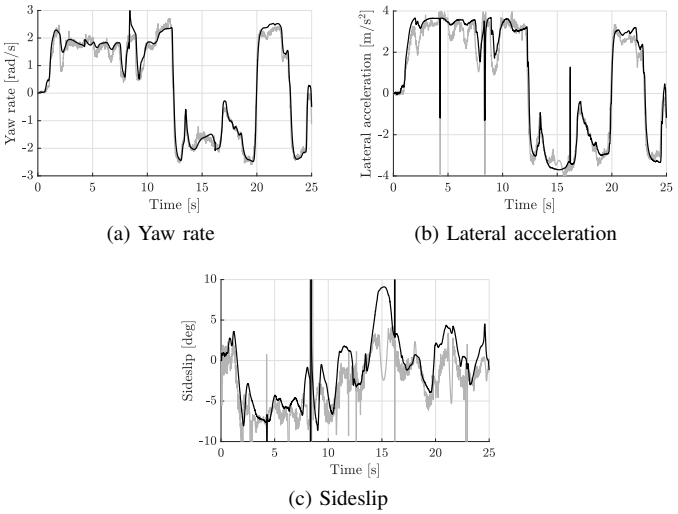

(a) Yaw rate (b) Lateral acceleration

(c) Sideslip

Fig. 7: Lateral dynamics (experimental data in grey, simulated data in black) in mixed trajectory experiment with drifting tyres.

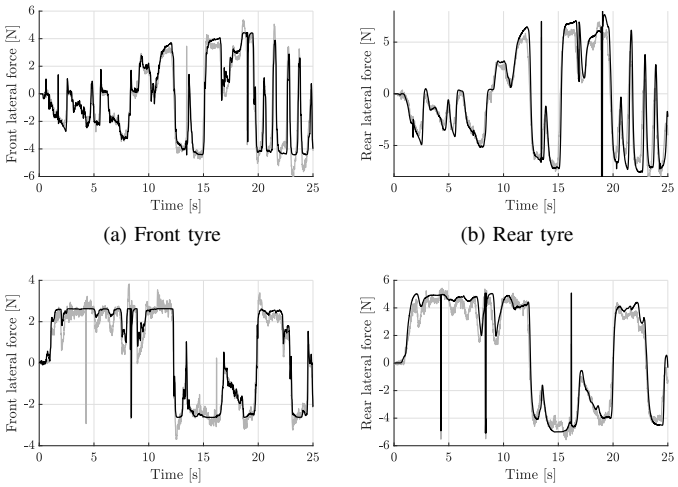

(a) Front tyre (b) Rear tyre

(c) Front tyre (d) Rear tyre

Fig. 8: Tyre lateral forces (experimental data in grey, simulated data in black) in mixed trajectory experiment with rubber (Figures 8a and 8b) and drifting (Figures 8c and 8d) tyres.

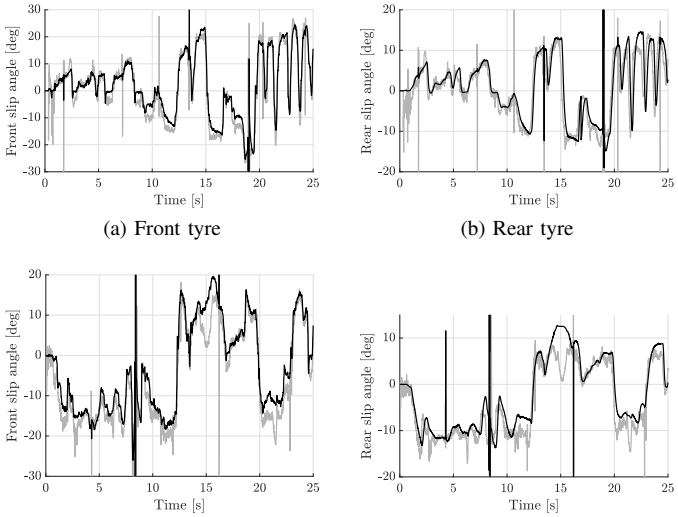

(a) Front tyre (b) Rear tyre

(c) Front tyre (d) Rear tyre

Fig. 9: Tyre slip angles (experimental data in grey, simulated data in black) in mixed trajectory experiment with rubber (Figures 9a and 9b) and drifting (Figures 9c and 9d) tyres.

the eight shaped trajectory is not able to persistently excite all system dynamics – see, e.g., Figures 10b and 10d showing an almost constant speed –, but it is a typical trajectory considered for drifting manoeuvres. As a consequence, this set of experiments aims on one side at showing a further validation of the identified parameters, on the other side at demonstrating that the identification algorithm is able to provide accurate results even in the case of a non-exciting trajectory.
An example of the input signals, i.e., vehicle speed and steer, is reported in Figures 10a and 10b for rubber tyres, and in Figures 10c and 10d for drifting tyres.

In this case, cornering stiffnesses and yaw inertia have been estimated considering the time interval $[5, 10]$ seconds for rubber and drifting tyres. The values of the identified parameters, reported in Table III, are the same as for the mixed trajectory experiment.

As for the mixed trajectory, a first validation (Figure 11) is based on a comparison between force-slip curves obtained from relation (12), using the estimated values of the cornering stiffnesses, and force and slip samples reconstructed from measurements. A second validation, instead, is based on a comparison between experimental and simulation data, where the second one are obtained simulating model (11)-(13) based on the values of the identified parameters. In particular, measurements related to the lateral dynamics (Figures 12 and 13), and reconstructed values of lateral forces (Figure 14) and slip

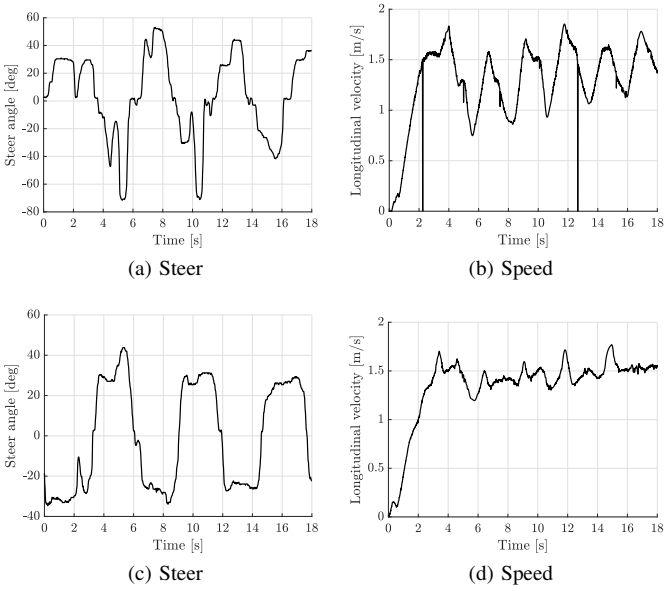

(a) Steer (b) Speed

(c) Steer (d) Speed

Fig. 10: Vehicle commands in eight shaped trajectory experiment with rubber (Figures 10a and 10b) and drifting (Figures 10c and 10d) tyres.

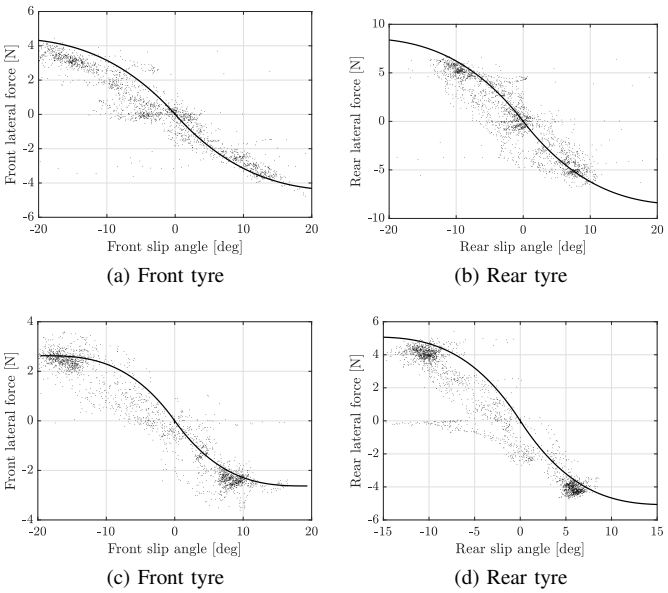

(a) Front tyre (b) Rear tyre

(c) Front tyre (d) Rear tyre

Fig. 11: Force-slip curve (estimated curve as a black solid line, experimental data as black dots) in eight shaped trajectory experiment with rubber (Figures 11a and 11b) and drifting (Figures 11c and 11d) tyres.

angles (Figure 15) are considered.
Though, as already mentioned, this trajectory, being more close to a realistic driving scenario, is not able to persistently excite all vehicle dynamics, it is still apparent that simulation and experimental results are in very good accordance.

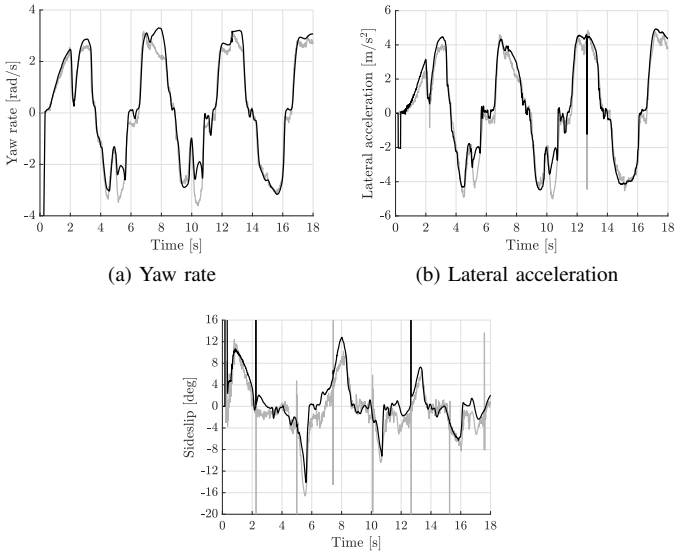

(a) Yaw rate (b) Lateral acceleration

(c) Sideslip

Fig. 12: Lateral dynamics (experimental data in grey, simulated data in black) in eight shaped trajectory experiment with rubber tyres.

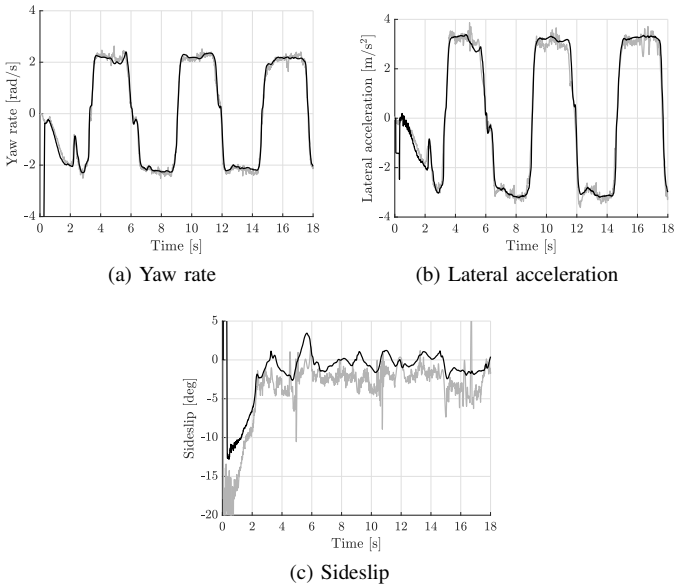

(a) Yaw rate (b) Lateral acceleration

(c) Sideslip

Fig. 13: Lateral dynamics (experimental data in grey, simulated data in black) in eight shaped trajectory experiment with drifting tyres.

Finally, as already mentioned, eight shaped trajectory can be used as a validation dataset to assess the performance of the identification algorithm. In fact, considering that the

TABLE IV: NMPE

	r	a_y	β	F_f	F_r	α_f	α_r
Rubber tyres	0.36	2.27	0.16	2.45	4.67	0.07	0.10
Drifting tyres	0.03	0.12	0.01	0.19	0.17	0.01	0.01

identification process yields the same values for the mixed and eight shaped trajectories, one can assume parameters in Table III have been identified with the mixed trajectory, and use the eight shaped trajectory as a validation dataset.

As a ground truth of cornering stiffness values is not available, the performance of the identification algorithm can be only indirectly assessed, considering the error in predicting the available measurements by simulating model (11)-(13) based on the identified parameters. In particular, for each variable y_i the Normalized Mean Prediction Error (NMPE) is considered, i.e.,

$$\text{NMPE}\left(y_i\right) = \frac{1}{N}\sum_{k=1}^{N}\left(\check{y}_i\left(t_k\right) - \hat{y}_i\left(t_k\right)\right)^2$$

where N is the number of samples, $\check{y}_i\left(t_k\right)$ and $\hat{y}_i\left(t_k\right)$ are the measured and simulated value of variable y_i at time instant t_k, respectively.

Table IV reports the values of the NMPE index for the eight shaped trajectory with rubber and drifting tyres related to the variables describing the lateral dynamics, that are directly measured, and the variables describing tyre-ground interaction, that are reconstructed from available measurements. The low values of NMPE on the whole validation dataset, either in the case of rubber and drifting tyres, confirm the validity of the proposed identification approach.

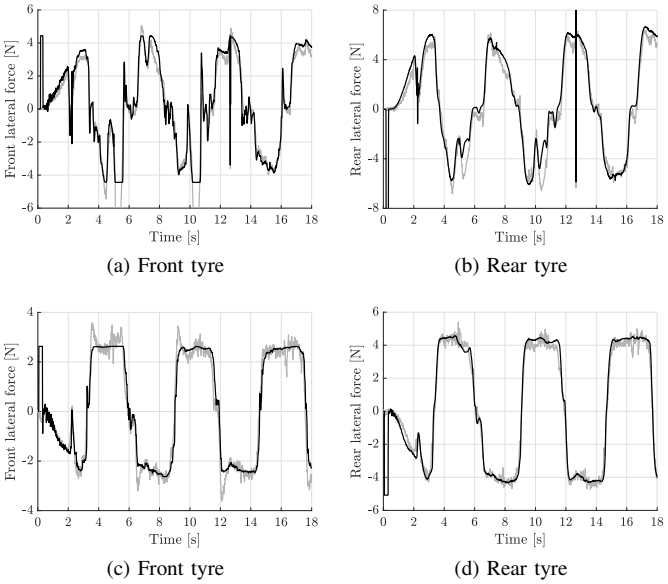

(a) Front tyre (b) Rear tyre

(c) Front tyre (d) Rear tyre

Fig. 14: Tyre lateral forces (experimental data in grey, simulated data in black) in eight shaped trajectory experiment with rubber (Figures 14a and 14b) and drifting (Figures 14c and 14d) tyres.

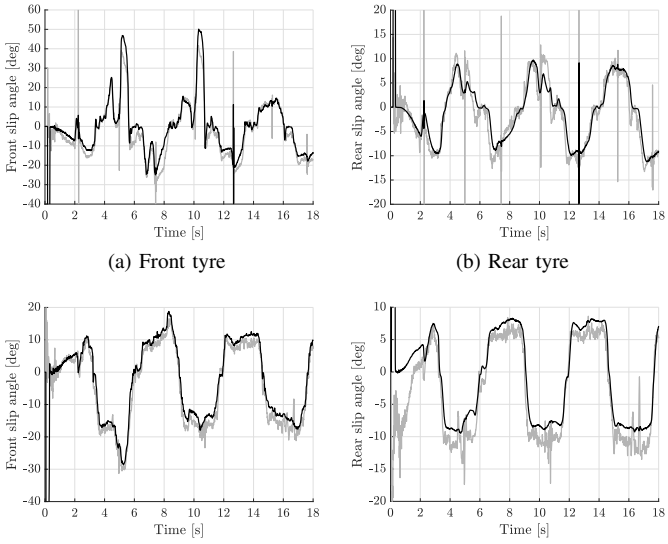

(a) Front tyre (b) Rear tyre

(c) Front tyre (d) Rear tyre

Fig. 15: Tyre slip angles (experimental data in grey, simulated data in black) in eight shaped trajectory experiment with rubber (Figures 15a and 15b) and drifting (Figures 15c and 15d) tyres.

C. Comparison with a different identification algorithm

In order to better assess the performance of the proposed algorithm, a comparison with a different approach to parameter identification of the vehicle lateral dynamics is here presented.

At the best of the authors' knowledge, no commonly accepted benchmark algorithm is available in the literature to assess the performance of state estimation and parameter identification approaches applied to vehicle lateral dynamics. Furthermore, according to the state-of-the-art presented in Section I, selecting the proper algorithm, i.e., an algorithm that should be able to

- support either a linear or nonlinear tyre model;
- solve simultaneously the state estimation and the parameter identification problem;
- support online estimation and parameter adaption running on a standard embedded device;

it is quite hard. For this reason, a parameter identification algorithm based on nonlinear optimisation [39], that has been already adopted for lateral vehicle dynamics identification [40], is here considered for the sake of comparison. This algorithm supports either a linear or nonlinear tyre model, and can solve almost simultaneously the state estimation and the parameter identification problem, but it cannot support online estimation as it involves a quite high computational burden. The ultimate goal of this comparison is thus to show that the quality of the results yielded by the proposed algorithm, e.g., in terms of NMPE value, are comparable to the ones obtained using a more accurate, but also computationally complex, algorithm.

The approach presented in [39], and already applied to the lateral vehicle dynamics identification problem in [40], is here used to estimate the front and rear cornering stiffness, and the yaw inertia, using the same measurements, i.e., yaw

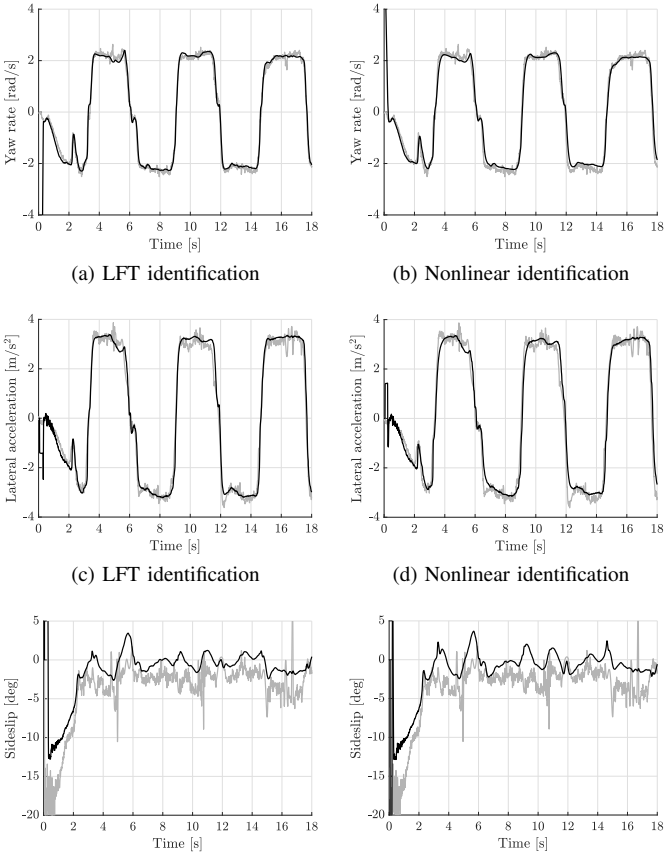

(a) LFT identification (b) Nonlinear identification

(c) LFT identification (d) Nonlinear identification

(e) LFT identification (f) Nonlinear identification

Fig. 16: Lateral dynamics (experimental data in grey, simulated data in black) in eight shaped trajectory experiment with drifting tyres, obtained with LFT (Figures 16a, 16c and 16e) and nonlinear (Figures 16b, 16d and 16f) identification algorithms.

rate r, lateral acceleration a_y, and sideslip angle β, the same time intervals, and the same experimental data adopted in Section V-B. The nonlinear optimisation problem has been started from one thousand different initial guesses, selected as the vertex of an equally spaced grid over the unknown space, characterised by $C_f \in [20, 30]$, $C_r \in [45, 55]$, and $I_z \in [0.028, 0.032]$.

Table V compares the values of the NMPE index for the two algorithms. According to these values, it is apparent that none of the two algorithms can be considered superior than the other one, as for some variables the LFT estimation outperforms, while for others the nonlinear estimation yields better results. In any case, the NMPE values are always so close that, from a practical point of view, the two identification algorithms can be considered equivalent, as it can be observed from the comparison of the estimated lateral dynamics quantities (Figure 16 and Figures 19a, 19b and 19g), tyre lateral forces (Figure 17 and Figures 19e and 19f), and slip angles (Figure 18 and Figures 19c and 19d).

In conclusion, the proposed identification algorithm exhibits the same performance of the nonlinear identification approach presented in [39], [40]. Despite this, the approach

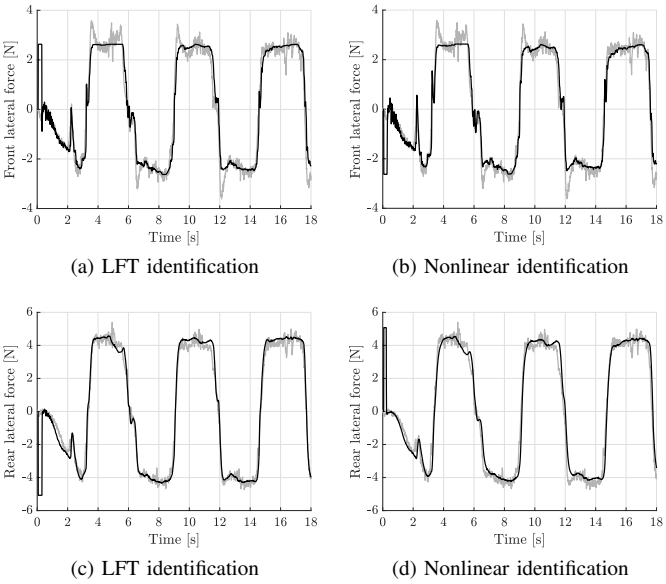

(a) LFT identification (b) Nonlinear identification

(c) LFT identification (d) Nonlinear identification

Fig. 17: Tyre lateral forces (experimental data in grey, simulated data in black) in eight shaped trajectory experiment with drifting tyres, obtained with LFT (Figures 18a and 18c) and nonlinear (Figures 18b and 18d) identification algorithms.

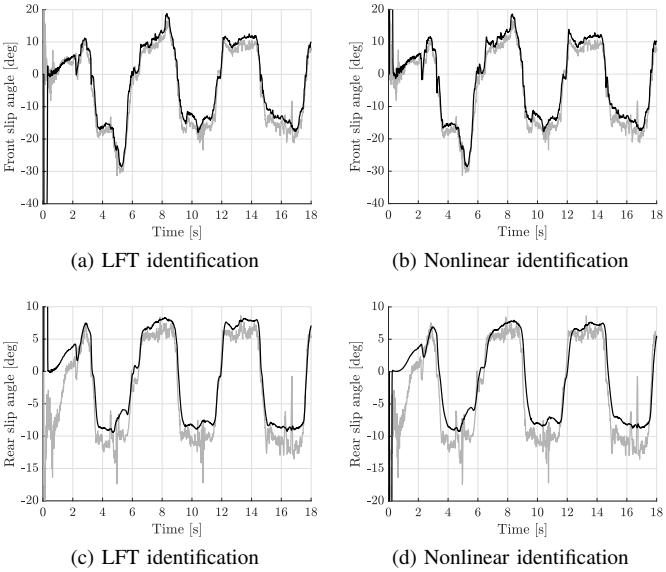

(a) LFT identification (b) Nonlinear identification

(c) LFT identification (d) Nonlinear identification

Fig. 18: Tyre slip angles (experimental data in grey, simulated data in black) in eight shaped trajectory experiment with drifting tyres, obtained with LFT (Figures 18a and 18c) and nonlinear (Figures 18b and 18d) identification algorithms.

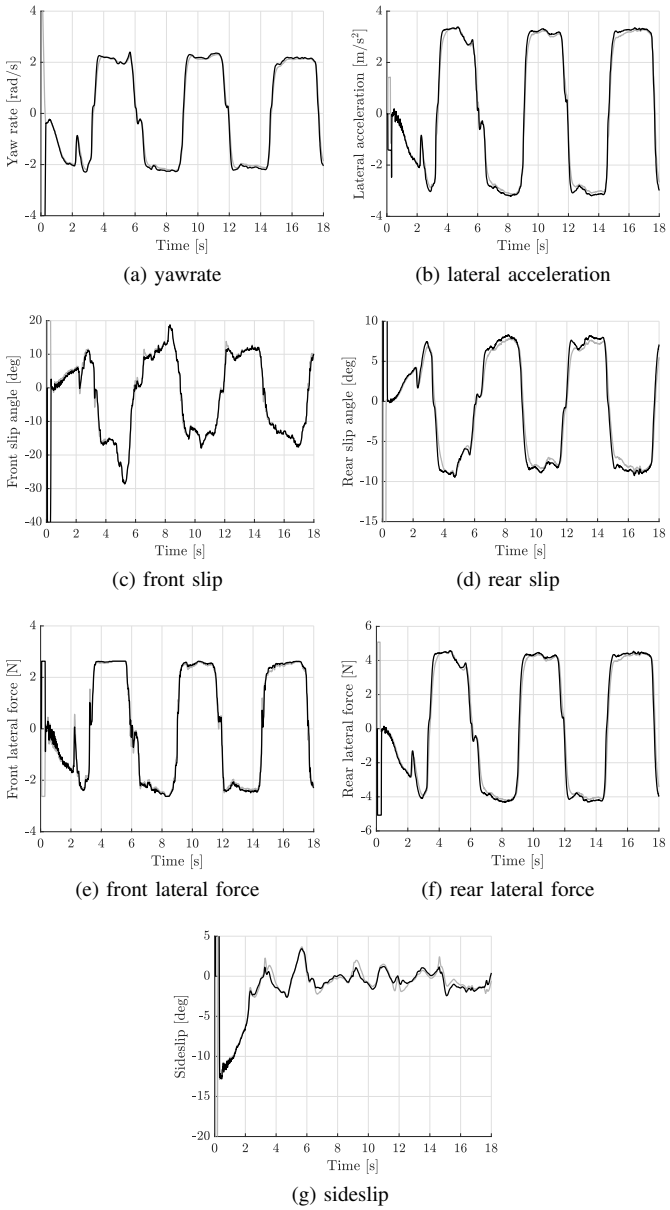

(a) yawrate (b) lateral acceleration

(c) front slip (d) rear slip

(e) front lateral force (f) rear lateral force

(g) sideslip

Fig. 19: Lateral dynamics, tyre lateral forces and slip angles in eight shaped trajectory experiment with drifting tyres, obtained with LFT (black solid line) and nonlinear identification algorithms (grey solid line).

here presented is computationally efficient, and can support online estimation and parameter adaption, it can be thus easily included in a real-time control algorithm. On the contrary, the nonlinear approach can be only used offline to analyse a previously recorded dataset using a batch approach.

VI. Conclusions

This paper presents a novel approach for lateral vehicle dynamics parameter identification and state estimation. The algorithm leverages on a LFT representation of vehicle and tyre models that allows to easily consider nonlinearities, and a simulation based identification procedure that, exploiting the properties of LFT representation, allows to develop a computationally efficient algorithm that can be easily translated in any programming language, and run on a standard embedded device for online identification. Furthermore, thanks to the adoption of nonlinear tyre models, like Fiala or Pacejka, the proposed algorithm can be used not only in standard driving conditions, but also at the limits of handling.

An extensive experimental campaign has been performed to validate the proposed identification approach, considering various trajectories executed on surfaces characterized by different static friction coefficients, and with different tyres. The results of two experiments characterized by a mixed trajectory, and two by an eight shaped trajectory, where for each trajectory one experiment is executed with drifting and one with rubber tyres, are presented, demonstrating the effectiveness of the algorithm in estimating the vehicle lateral dynamics.

Considering that in some applications load transfer can play an important role in tyre behaviour, but it can significantly increase the complexity of the identification problem, an extension of the methodology here proposed, that allows to take load transfer into account, will be considered as a future work.

TABLE V: NMPE comparison

	LFT identification		Nonlinear identification	
	Rubber tyres	Drifting tyres	Rubber tyres	Drifting tyres
r	0.36	0.03	1.23	0.05
a_y	2.27	0.12	0.92	0.19
β	0.16	0.01	0.18	0.01
F_f	2.45	0.19	2.31	0.15
F_r	4.67	0.17	2.10	0.33
α_f	0.07	0.01	0.08	0.01
α_r	0.10	0.01	0.08	0.01

Appendix A
LFT single-track model matrices

The sixteen constant matrices that allow to express the single-track model in LFT formulation are here reported:

$$\mathbf{A} = \begin{bmatrix} 0 & 0 \\ 0 & 0 \end{bmatrix} \qquad \mathbf{B}_1 = \begin{bmatrix} 1 & 1 & 0 \\ 0 & 0 & 1 \end{bmatrix}$$

$$\mathbf{B}_2 = \begin{bmatrix} 0 & 0 & 0 & -1 & 0 \\ 0 & 0 & 0 & 0 & -\frac{b}{a} \end{bmatrix} \qquad \mathbf{B}_3 = \begin{bmatrix} 0 & 0 \\ 0 & 0 \end{bmatrix}$$

$$\mathbf{C}_1 = \begin{bmatrix} 0 & 0 \\ 0 & 0 \\ 0 & 0 \end{bmatrix} \qquad \mathbf{D}_{11} = \begin{bmatrix} 0 & 0 & 0 \\ 0 & 0 & 0 \\ 0 & 0 & 0 \end{bmatrix}$$

$$\mathbf{D}_{12} = \begin{bmatrix} 0 & 1 & 0 & 0 & 0 \\ 0 & 0 & 1 & 0 & 0 \\ 0 & a & 0 & 0 & 0 \end{bmatrix} \qquad \mathbf{D}_{13} = \begin{bmatrix} 0 & 0 \\ 0 & 0 \\ 0 & 0 \end{bmatrix}$$

$$\mathbf{C}_2 = \begin{bmatrix} 1 & 0 \\ 0 & 1 \\ 0 & 0 \\ 0 & 0 \\ 0 & 0 \\ 0 & 0 \\ 0 & 0 \\ 0 & 0 \end{bmatrix} \qquad \mathbf{D}_{21} = \begin{bmatrix} 0 & 0 & 0 \\ 0 & 0 & 0 \\ 1 & 0 & 0 \\ 0 & 1 & 0 \\ 0 & 0 & 1 \\ 0 & 0 & 0 \\ 0 & 0 & 0 \\ 0 & 0 & 0 \end{bmatrix}$$

$$\mathbf{D}_{22} = \begin{bmatrix} 0 & 0 & 0 & 0 & 0 \\ 0 & 0 & 0 & 0 & 0 \\ 0 & 0 & 0 & 0 & 0 \\ 0 & 0 & 0 & 0 & 0 \\ 0 & 0 & 0 & 0 & 0 \\ 1 & 0 & 0 & 0 & 0 \\ 0 & 0 & 0 & 0 & 0 \\ 0 & 0 & 0 & 0 & 0 \end{bmatrix} \qquad \mathbf{D}_{23} = \begin{bmatrix} 0 & 0 \\ 0 & 0 \\ 0 & 0 \\ 0 & 0 \\ 0 & 0 \\ 0 & 0 \\ 1 & 0 \\ 0 & 1 \end{bmatrix}$$

$$\mathbf{C}_3 = \begin{bmatrix} 0 & 1 \\ 0 & 0 \\ 0 & 0 \end{bmatrix} \qquad \mathbf{D}_{31} = \begin{bmatrix} 0 & 0 & 0 \\ 1 & 1 & 0 \\ 0 & 0 & 0 \end{bmatrix}$$

$$\mathbf{D}_{32} = \begin{bmatrix} 0 & 0 & 0 & 0 & 0 \\ 0 & 0 & 0 & 0 & 0 \\ 1 & 0 & 0 & 0 & 0 \end{bmatrix} \qquad \mathbf{D}_{33} = \begin{bmatrix} 0 & 0 \\ 0 & 0 \\ 0 & 0 \end{bmatrix}$$

APPENDIX B
LFT SINGLE-TRACK MODEL WITH PACEJKA MODEL

The same single-track motion model introduced in Section III is here considered

$$\begin{aligned} m\dot{v}_y &= F_f + F_r - m v_x r \\ I_z \dot{r} &= a F_f - b F_r \\ \dot{\psi} &= r \end{aligned}$$

but now the lateral forces are related to the slip angles using the Pacejka tyre model [41]

$$\begin{aligned} F_\star = D_\star \sin\{C_\star \arctan[B_\star \alpha_\star \\ - E_\star (B_\star \alpha_\star - \arctan(B_\star \alpha_\star))]\} \end{aligned}$$

where "$\star$" stands for "f" or "r", $B_\star$, $C_\star$, $D_\star$ and $E_\star$ are the coefficients of the magic formula, and $\alpha_\star$ are the slip angles defined as in (13).

This model can be written in the general form (1) by defining the same state, input and output vectors as in (15), while considering the parameter vector

$$\boldsymbol{\delta} = \begin{bmatrix} \dfrac{D_f}{m} & \dfrac{D_r}{m} & \dfrac{D_f}{I_z} & B_f & C_f & E_f & B_r & C_r & E_r \end{bmatrix}^T$$

obtaining the LFT reformulation given by

$$\dot{\mathbf{x}} = \begin{bmatrix} w_1 + w_2 - \zeta_{10} \\ \dfrac{b}{a} w_3 - \zeta_{11} \end{bmatrix} \qquad \mathbf{z} = \begin{bmatrix} \zeta_2 \\ \zeta_3 \\ a\zeta_2 \\ \zeta_4 \\ \zeta_5 \\ \zeta_6 \\ \zeta_7 \\ \zeta_8 \\ \zeta_9 \end{bmatrix} \qquad \mathbf{w} = \begin{bmatrix} z_1\delta_1 \\ z_2\delta_2 \\ z_3\delta_3 \\ z_4\delta_4 \\ z_5\delta_5 \\ z_6\delta_6 \\ z_7\delta_7 \\ z_8\delta_8 \\ z_9\delta_9 \end{bmatrix}$$

$$\boldsymbol{\omega} = \begin{bmatrix} x_1 \\ x_2 \\ w_1 \\ w_2 \\ w_3 \\ \zeta_1 \\ u_1 \\ u_2 \\ w_5 \\ w_8 \\ w_4 \\ w_6 \\ w_7 \\ w_9 \end{bmatrix} \qquad \boldsymbol{\zeta} = \begin{bmatrix} \arctan \dfrac{\omega_1}{\omega_7} \\ \sin(\omega_9) \\ \sin(\omega_{10}) \\ -\omega_6 - a\dfrac{\omega_2}{\omega_7} + G\omega_8 \\ \arctan(\omega_{11} - \omega_{12}) \\ \omega_{11} - \arctan(\omega_{11}) \\ -\omega_6 + b\dfrac{\omega_2}{\omega_7} \\ \arctan(\omega_{13} - \omega_{14}) \\ \omega_{13} - \arctan(\omega_{13}) \\ \omega_2\omega_7 \\ \dfrac{\omega_4\omega_5}{\omega_3} \end{bmatrix}$$

$$\mathbf{y} = \begin{bmatrix} x_2 \\ w_1 + w_2 \\ \zeta_1 \end{bmatrix}$$

REFERENCES

[1] R. Rajamani, G. Phanomchoeng, D. Piyabongkarn, and J. Lew, "Algorithms for real-time estimation of individual wheel tire-road friction coefficients," *IEEE/ASME Transactions on Mechatronics*, vol. 17, no. 6, pp. 1183–1195, 2012.

[2] R. Rajamani, *Vehicle Dynamics and Control*. Springer, 2011.

[3] R. Rajamani, N. Piyabongkarn, J. Lew, K. Yi, and G. Phanomchoeng, "Tire-road friction-coefficient estimation," *IEEE Control Systems Magazine*, vol. 30, no. 4, pp. 54–69, 2010.

[4] Jin-Oh Hahn, R. Rajamani, and L. Alexander, "GPS-based real-time identification of tire-road friction coefficient," *IEEE Transactions on Control Systems Technology*, vol. 10, no. 3, pp. 331–343, 2002.

[5] L. Ruotsalainen, V. Renaudin, L. Pei, M. Piras, J. Marais, E. Cavalheri, and S. Kaasalainen, "Toward autonomous driving in arctic areas," *IEEE Intelligent Transportation Systems Magazine*, vol. 12, no. 3, pp. 10–24, 2020.

[6] M. Sharifzadeh, A. Senatore, A. Farnam, A. Akbari, and F. Timpone, "A real-time approach to robust identification of tyre-road friction characteristics on mixed-μ roads," *Vehicle System Dynamics*, vol. 57, no. 9, pp. 1338–1362, 2019.

[7] Y.-W. Liao and F. Borrelli, "An adaptive approach to real-time estimation of vehicle sideslip, road bank angles, and sensor bias," *IEEE Transactions on Vehicular Technology*, vol. 68, no. 8, pp. 7443–7454, 2019.

[8] A. J. Tuononen, M. Ovaska, and A. Niskanen, "Review on tire-road-friction potential estimation technologies," in *International Symposium on Dynamics of Vehicles on Roads and Tracks*, 2019, pp. 1027–1032.

[9] M. Arndt, E. L. Ding, and T. Massel, "Identification of cornering stiffness during lane change maneuvers," in *IEEE International Conference on Control Applications*, vol. 1, 2004, pp. 344–349.

[10] B. Chen, B. Luan, and K. Lee, "Design of lane keeping system using adaptive model predictive control," in *IEEE International Conference on Automation Science and Engineering (CASE)*, 2014, pp. 922–926.

[11] S. Sivaramakrishnan, "Simultaneous identification of tire cornering stiffnesses and vehicle center of gravity," in *American Control Conference*, 2008, pp. 2846–2851.

[12] M. Akar and A. D. Dere, "A switching rollover controller coupled with closed-loop adaptive vehicle parameter identification," *IEEE Transactions on Intelligent Transportation Systems*, vol. 15, no. 4, pp. 1579–1585, 2014.

[13] K. Han, M. Choi, and S. B. Choi, "Estimation of the tire cornering stiffness as a road surface classification indicator using understeering characteristics," *IEEE Transactions on Vehicular Technology*, vol. 67, no. 8, pp. 6851–6860, 2018.

[14] H. Jung and S. B. Choi, "Real-time individual tire force estimation for an all-wheel drive vehicle," *IEEE Transactions on Vehicular Technology*, vol. 67, no. 4, pp. 2934–2944, 2018.

[15] J. Stephant and A. Charara, "Observability matrix and parameter identification: application to vehicle tire cornering stiffness," in *IEEE Conference on Decision and Control*, 2005, pp. 6734–6739.

[16] D. M. Bevly, J. Ryu, and J. C. Gerdes, "Integrating ins sensors with gps measurements for continuous estimation of vehicle sideslip, roll, and tire cornering stiffness," *IEEE Transactions on Intelligent Transportation Systems*, vol. 7, no. 4, pp. 483–493, 2006.

[17] G. Baffet, A. Charara, and D. Lechner, "Estimation of vehicle sideslip, tire force and wheel cornering stiffness," *Control Engineering Practice*, vol. 17, no. 11, pp. 1255–1264, 2009.

[18] N. Liu and A. G. Alleyne, "Iterative learning identification applied to automated off-highway vehicle," *IEEE Transactions on Control Systems Technology*, vol. 22, no. 1, pp. 331–337, 2014.

[19] W. Chen, D. Tan, and L. Zhao, "Vehicle sideslip angle and road friction estimation using online gradient descent algorithm," *IEEE Transactions on Vehicular Technology*, vol. 67, no. 12, pp. 11 475–11 485, 2018.

[20] F. Naets, S. van Aalst, B. Boulkroune, N. E. Ghouti, and W. Desmet, "Design and experimental validation of a stable two-stage estimator for automotive sideslip angle and tire parameters," *IEEE Transactions on Vehicular Technology*, vol. 66, no. 11, pp. 9727–9742, 2017.

[21] M. Acosta, S. Kanarachos, and M. E. Fitzpatrick, "Robust virtual sensing for vehicle agile manoeuvring: A tyre-model-less approach," *IEEE Transactions on Vehicular Technology*, vol. 67, no. 3, pp. 1894–1908, 2018.

[22] Jin-Oh Hahn, R. Rajamani, and L. Alexander, "GPS-based real-time identification of tire-road friction coefficient," *IEEE Transactions on Control Systems Technology*, vol. 10, no. 3, pp. 331–343, 2002.

[23] M. Choi, J. J. Oh, and S. B. Choi, "Linearized recursive least squares methods for real-time identification of tire-road friction coefficient," *IEEE Transactions on Vehicular Technology*, vol. 62, no. 7, pp. 2906–2918, 2013.

[24] C. Kim, J. Hahn, K. Hong, and W. Yoo, "Estimation of tire-road friction based on onboard 6-dof acceleration measurement," *IEEE Transactions on Vehicular Technology*, vol. 64, no. 8, pp. 3368–3377, 2015.

[25] R. Wang and J. Wang, "Tire-road friction coefficient and tire cornering stiffness estimation based on longitudinal tire force difference generation," *Control Engineering Practice*, vol. 21, no. 1, pp. 65–75, 2013.

[26] A. Lopes and R. E. Araújo, "Vehicle lateral dynamic identification method based on adaptive algorithm," *IEEE Open Journal of Vehicular Technology*, vol. 1, pp. 267–278, 2020.

[27] G. Baffet, A. Charara, and G. Dherbomez, "An observer of tire-road forces and friction for active security vehicle systems," *IEEE/ASME Transactions on Mechatronics*, vol. 12, no. 6, pp. 651–661, 2007.

[28] L. H. Lee and K. Poolla, "Identification of Linear Parameter-Varying Systems Using Nonlinear Programming," *Journal of Dynamic Systems, Measurement, and Control*, vol. 121, pp. 71–78, 1999.

[29] F. Demourant and G. Ferreres, "Closed loop identification of a LFT model," *Journal Européen des Systémes Automatisés*, vol. 36, no. 3, pp. 449–464, 2002.

[30] K. Hsu, T. Vincent, G. Wolodkin, S. Rangan, and K. Poolla, "An LFT approach to parameter estimation," *Automatica*, vol. 44, no. 12, pp. 3087–3092, 2008.

[31] A. Della Bona, G. Ferretti, E. Ficara, and F. Malpei, "LFT modelling and identification of anaerobic digestion," *Control Engineering Practice*, vol. 36, pp. 1–11, 2015.

[32] L. Ljung, *System Identification: Theory for the User*. Prentice Hall, 1999.

[33] N. Kapania and J. Gerdes, "Design of a feedback-feedforward steering controller for accurate path tracking and stability at the limits of handling," *Vehicle System Dynamics*, vol. 53, no. 12, pp. 1687–1704, 2015.

[34] L. Bascetta, M. Baur, and G. Ferretti, "A simple and reliable technique to design kinematic-based sideslip estimators," *Control Engineering Practice*, vol. 96, pp. 104–317, 2020.

[35] A. Liniger, A. Domahidi, and M. Morari, "Optimization-based autonomous racing of 1:43 scale RC cars," *Optimal Control Applications and Methods*, vol. 36, no. 5, pp. 628–647, 2015.

[36] G. Williams, P. Drews, B. Goldfain, J. M. Rehg, and E. A. Theodorou, "Aggressive driving with model predictive path integral control," in *IEEE International Conference on Robotics and Automation*, 2016, pp. 1433–1440.

[37] S. Brennan and A. Alleyne, "Using a scale testbed: controller design and evaluation," *IEEE Control Syst. Mag.*, vol. 21, no. 3, pp. 15–26, 2001.

[38] P. Hoblet, R. T. O'Brien, and J. A. Piepmeier, "Scale-model vehicle analysis for the design of a steering controller," in *Southeastern Symposium on System Theory*, 2003, pp. 201–205.

[39] L. Fagiano, M. Lauricella, D. Angelosante, and E. Ragaini, "Identification of induction motors using smart circuit breakers," *IEEE Transactions on Control Systems Technology*, no. 99, pp. 1–9, 2018.

[40] M. Baur and L. Bascetta, "An experimentally validated lqr approach to autonomous drifting stabilization," in *18th European Control Conference (ECC)*, 2019, pp. 732–737.

[41] P. H.B., *Tyre and vehicle dynamics*, 2nd ed. Butterworth-Heinemann, Oxford, 2006.

Luca Bascetta Luca Bascetta was born in Milano (Italy) in 1974. He received the Laurea degree cum laude in Computer Science Engineering and the Doctorate degree in Information Technology in 1999 and 2004, respectively, both from Politecnico di Milano, Italy. From 2015 he has been Associate Professor in Automatic Control and Control of Mobile Robots at the School of Industrial and Information Engineering of Politecnico His research interests include autonomous vehicles, robotics, visual servoing and all the problems related to motion control in general. Professor Bascetta is a senior member of IEEE Robotics and Automation Society since 2017.

Gianni Ferretti Gianni Ferretti was born in Cremona (Italy) in 1962. He received the "Laurea" degree in Electronics Engineering in 1987 from Politecnico di Milano. From 1990 to 1998 he was Assistant Professor at the Department of Electronics and Computer Science of Politecnico di Milano and in 1994 he was a visiting researcher at the Laboratoire dAutomatique de Grenoble. From 1998 to 2005 he was Associate Professor at Politecnico di Milano where he is currently Full Professor in Automatic Control. He is Vice Rector for the Cremona campus of Politecnico di Milano and teaches Fundamentals of Automatic Control and Simulation Techniques and Tools. His principal research interests are: control of servomechanisms, modelling and simulation of mechatronic systems, force/position control of robots, modelling and simulation of automotive systems, modelling and control of biogas power plants. He is coauthor of more than 100 papers, most of which published in international journals or presented in international conferences, and was involved in many research projects with industries and institutions.